Click Here for Full Article

Effects of dead time losses on terrestrial gamma ray flash measurements with the Burst and Transient Source Experiment

T. Gjesteland,[1] N. Østgaard,[1] P. H. Connell,[2] J. Stadsnes,[1] and G. J. Fishman[3]

[1] Measurements from the Burst and Transient Source Experiment (BATSE) instrument on the Compton Gamma Ray Observatory (CGRO) are the only ones where characteristics of single terrestrial gamma ray flashes (TGFs) have been obtained thus far. However, it has been reported that the measurements suffer from significant dead time losses which complicates the analysis and raises question about earlier BATSE studies. These losses are due to the high-intensity flux combined with limitations of the time resolution of the instrument. Since these losses will affect both the spectrum and the temporal distribution of the individual TGFs, results based on BATSE data need to be revisited, including our own. We have therefore developed a Monte Carlo method to study the effects of these dead time losses. We show that the energy spectrum of TGFs becomes softer as the dead time losses increase. We also show that the time delay between the light curves of hard ($E > 300$ keV) and soft ($E < 300$ keV) photons increases significantly as the dead time losses increase. The Monte Carlo approach also enables us to identify the BATSE TGFs where the dead time effects can be corrected. These are the short-duration single-peaked TGFs. Without correcting for dead time losses we find that these short single-peak TGFs have a softer energy spectrum and larger time delay than the multipeaked TGFs. After correcting for dead time losses we perform a new analysis of production altitudes and find that the production altitude is reduced compared to analysis without dead time losses. The new production altitudes combined with dead time losses are also consistent with the apparent large time delays. Our method gives consistent results regarding production altitude and time delays and indicates that the corrected TGF intensities measured by BATSE are 3 to 4 times brighter than the uncorrected measurements would indicate. We also show that the production mechanism of these TGFs has a typical duration of 250 μs.

1. Introduction

[2] Terrestrial gamma ray flashes (TGFs) were discovered by the Burst and Transient Source Experiment (BATSE) on board the Compton Gamma Ray Observatory (CGRO) [*Fishman et al.*, 1994]. They were found to be short (~1 ms) gamma bursts related to thunderstorms. Triangulation of ELF/VLF radio atmospherics (sferics) from lightning have shown that TGF are indeed related to lightning [*Inan et al.*, 1996; *Cummer et al.*, 2005; *Inan et al.*, 2006; *Cohen et al.*, 2006; *Stanley et al.*, 2006]. New observations of TGFs have been provided by the Reuven Ramaty High Energy Solar Spectroscopic Imager (RHESSI) [*Smith et al.*, 2005], showing gamma photons which energy were up to 20 MeV.

[3] While the production mechanism of TGF is still not determined, they are assumed to be bremsstrahlung from a relativistic runaway electric avalanche (RREA) [*Roussel-Dupre et al.*, 1994; *Gurevich and Zybin*, 2001]. TGF was first assumed to be associated with red sprites at 30–80 km altitude [*Nemiroff et al.*, 1997]. Thus, a quasi-electrostatic (QES) field [*Lehtinen et al.*, 1996] and electromagnetic pulses (EMPs) [*Inan and Lehtinen*, 2005] were suggested to explain how a relativistic runaway breakdown process could occur at these altitudes. However, other studies have suggested that leaders and streamers could be a source of runaway electrons [*Moss et al.*, 2006; *Chanrion and Nubert*, 2008] indicating a much lower production altitude. Recently, simulations by *Carlson et al.* [2009] found that RREA in lightning leaders can produce TGFs, implying a production altitude within thunder clouds.

[4] Because of the attenuation of X-rays and gamma rays propagating through the atmosphere, spectral measurements from BATSE and RHESSI are used to determine the production altitude of TGFs. *Dwyer and Smith* [2005] used a

[1]Department of Physics and Technology, University of Bergen, Bergen, Norway.
[2]Institute of Mechanical Science, University of Valencia, Valencia, Spain.
[3]NASA Marshall Space Flight Center, Huntsville, Alabama, USA.

superposition of all the RHESSI TGFs to show that a simulated TGF produced at 15–21 km altitude could best reproduce the RHESSI spectrum. This average value of production altitude based on superposed RHESSI spectrum was also reported by *Carlson et al.* [2007]. *Carlson et al.* [2007] also found the BATSE measurements fit a production altitude of 15 km. A production altitude of ~15 km is consistent with tropical thunderstorm [*Williams et al.*, 2006]. *Østgaard et al.* [2008] used a different approach in the analysis of the BATSE TGFs. Instead of using a superposition of all events, *Østgaard et al.* [2008] analyzed each individual TGF and concluded that a majority were produced at low altitude (10 to 20 km) while a significant portion was produced at higher altitude, i.e., 30 to 40 km.

[5] Since then it has been shown that the BATSE instrument suffers from a significant dead time problem [*Grefenstette et al.*, 2008], i.e., that the read-out electronics of the BATSE instruments are not fast enough to count all the scintillation pulses from the detector material (NaI). In most cases this is an effect that can be corrected for, unless the system is paralyzed. On the basis of preflight data, *Grefenstette et al.* [2008] showed that BATSE was indeed a paralyzable detector. As the time delays observed by BATSE were systematically longer than what can be explained by Compton scattering, they claimed that the dead time losses in the detector could account for this extra time delay. They also showed that BATSE TGFs, which suffer from significant dead time losses, show a softer energy spectrum than the true spectrum.

[6] An analysis of the temporal behavior of TGFs by *Feng et al.* [2002] found the low-energy photons (25 keV < E < 110 keV) to have a ~100 μs delay compared to the high-energy photons (E > 110 keV). *Østgaard et al.* [2008] found that observed time delays can be explained qualitatively by Compton scattering effects of the X-rays as they propagate through the atmosphere. However, when we looked in more detail we found that the Compton scattering effect alone could not account for the entire time delay, which supports the hypothesis of dead time losses being responsible for the large time delays [*Grefenstette et al.*, 2008].

[7] Furthermore, as long as the effect of dead time losses has not been addressed it can be argued that all temporal and spectral results based on BATSE measurements without taking dead time effects into account are questionable.

[8] Because of the long trigger window (64 ms), a short event such as a TGF (which typically lasts 1 ms) needs to be very intense to cause a trigger. Several of the BATSE TGFs contain several peaks, each lasting approx 1 ms. On the basis of the same argument, we would assume that single-peaked TGFs suffer from more dead time losses than the multipeaked TGFs. In the work of *Østgaard et al.* [2008], a significant portion of the TGFs were found to be produced at 30 to 40 km altitude, most of them being short-duration single-peaked TGFs.

[9] In this study we present a Monte Carlo simulation of the BATSE detector and read-out electronics. We follow each photon from its entrance into the detector material using the Detector Response Matrix (DRM) to produce an electric pulse. Then we carefully model the read-out electronics with its characteristic decay time and reset level to obtain the measured count rates. We will show how we can determine whether the detector is paralyzed or not and why

the dead time effects can be corrected for in detected single-peaked TGFs. This approach enables us to obtain new estimates of production altitude which is consistent with the measured time delays. The paper is organized as follows: First, a section describing the method applied to one TGF (section 2), then a section presenting the results for five single TGFs (section 3), followed by discussion and summary sections (sections 4 and 5).

2. Method

[10] To analyze the BATSE measurements, we have developed a Monte Carlo simulation where the input is the photon distribution in time and energy (spectrum). The Detector Response Matrix (DRM) gives the conversion of photons to electronic pulses. The readout electronics are then modeled with its characteristic decay time and reset level which define the dead time for different incoming flux levels. This enables us to estimate the measured count rates of the detector. Our tools in this analysis are (1) a Monte Carlo input-spectrum, with assumptions about initial spectral and spatial distribution for various production altitudes; (2) the Detector Response Matrix; and (3) Monte Carlo simulation of the dead time losses. The Monte Carlo simulation of photons propagating trough the atmosphere is the same as that described by *Østgaard et al.* [2008] with the following initial assumptions:

[11] 1. A photon energy spectrum on the form

$$F(E) = E^{-\gamma} \exp \frac{-E}{10 \text{ MeV}}. \tag{1}$$

[12] 2. A beamed (half-angle 1°) or isotropic cone (half-angle 50°) distribution.

[13] 3. Discrete production altitude ranging from 10 km to 30 km.

[14] In the work of *Østgaard et al.* [2008], the energy spectrum was on the form $F(E) = E^{-\gamma}$, and the isotropic cone half-angle was 20°. The energy spectrum is modified with an exponential term (1) to avoid a sharp cut off at high energies, which is closer to the expected bremsstrahlung spectrum from the runaway electrons [*Dwyer and Smith*, 2005]. The broadness of the cone is here set to 50°, which is wider than given by *Østgaard et al.* [2008] where the half-angle was 20°. The rational for using a wider cone angle is that BATSE will then be inside that cone for all the TGFs we analyze in this paper. The wider beam is also similar to results from *Dwyer and Smith* [2005] and *Carlson et al.* [2007], who found that a wider beam (half-angle 45°) fits the RHESSI data for a 15 km source altitude.

[15] To analyze the production altitude and the TGF's temporal behavior, we present this method in seven steps using TGF 2955 as an example. The initial assumptions for our simulated TGF are a beamed distribution produced at 20 km altitude and an initial energy spectrum on the form of equation (1), where $\gamma = 1.0$, which is what one expects for a bremsstrahlung spectrum.

[16] Step 1: Determine the duration of the TGF production process. Since the dead time losses depend on both the total number of photons, their energy, and how they are distributed in time, the temporal properties of the TGF production
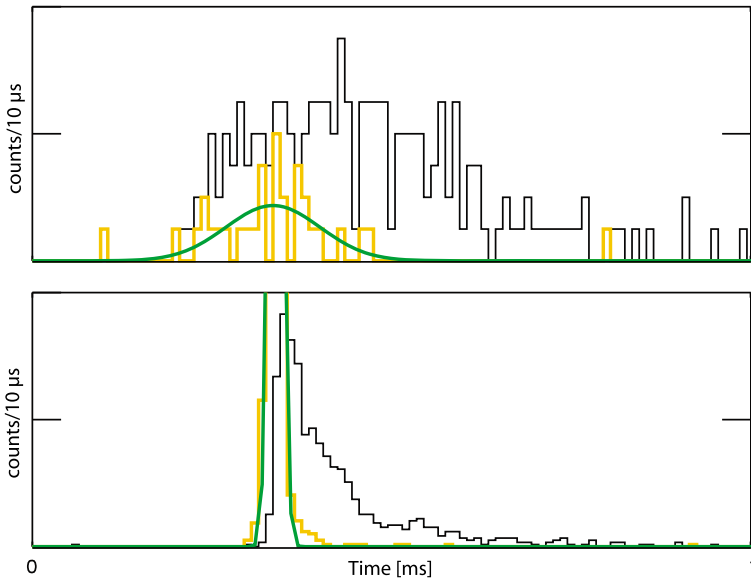
Figure 1. (top) Light curve of BATSE TGF 2955. (bottom) Light curve from MC simulation. The light curve of all photons is black, and the light curve of the hard photons (E > 300 keV) is orange.

mechanism must be included in the simulations. From our simulations of X-ray propagation through the atmosphere we know that most of the low-energy photons that escape the atmosphere are originally high-energy photons that are Compton scattered in the atmosphere and reduced in energy [*Østgaard et al.*, 2008]. This scattering process makes their travel path longer which again results in a dispersion. On the other hand, the high-energy photons that escape the atmosphere are hardly scattered and therefore travel almost directly from their origin up to satellite altitudes. Assuming no dispersion in the emitting process, we can assume that the temporal distribution of hard photons (E > 300 keV) measured by BATSE reflects the temporal distribution of the production mechanism with only a small dispersion effect. However, from our Monte Carlo model of X-rays through the atmosphere we can find the dispersion due to Compton scattering for photons E > 300 keV, which can be subtracted from the duration of the measured E > 300 keV photons. In Figure 1 (top) the light curve of TGF 2955 is black, and the light curve of hard photons (channel 4, E > 300 keV) is orange, with a green Gauss-fitted curve. Figure 1 (bottom) shows the total and the hard light curve from our simulations. All the photons start at the same time at the TGF's production altitude in our simulation. The duration of the hard light curves is determined as ±2σ of the Gaussian-fitted curves. While the duration of high-energy photons in our simulation only lasts 10 μs, the hard light curve of BATSE TGF 2955 lasts 260 μs. For the duration of the TGF production mechanism we therefore use Gaussian temporal behavior which is 250 μs within ±2σ. As mentioned above, we use a photon distribution escaping the atmosphere from a production altitude of 20 km. For each of these photons a

Gaussian-distributed random Δt between 0 and 250 μs is added to the time delays we already have from Compton scattering to have the most realistic distribution of photons in both energy and time.

[17] Step 2: Determine the zenith angle or angle of entrance to the detector. The relative total counts in the four Large Area Detectors (LADs) that have most counts are used to estimate the zenith angle. Of the escaping photons in our simulation we use the photons that would hit BATSE at the calculated zenith angle ±5°

[18] Step 3: Convert from photons to pulses in the detector material. The zenith angle and the DRM will give us the effective detecting area for each of the LADs. DRM give us then to covert the incoming photons to pulses in the four BATSE discriminator levels. For various numbers of incoming photons we use the DRM to determine whether or not the photon will interact with the LAD, which discriminator will respond to and produce a pulse. The four discriminators have the following energy ranges: 25 to 60 keV, 60 to 110 keV, 110 to 320 keV, and >320 keV.

[19] Step 4: Convert from pulse to count. If the pulses in the detector are coming faster than the electronics can register them, the detector will suffer from dead time losses. *Grefenstette et al.* [2008] showed that BATSE has a dead time given by

$$\tau \sim \alpha \ln \frac{E_p}{E_0}, \qquad (2)$$

where α is the signal decay time, E_p is the energy of the photon, and E_0 is the reset level of the detector. A photon hitting a LAD will produce a pulse, V_p, that rises in a very
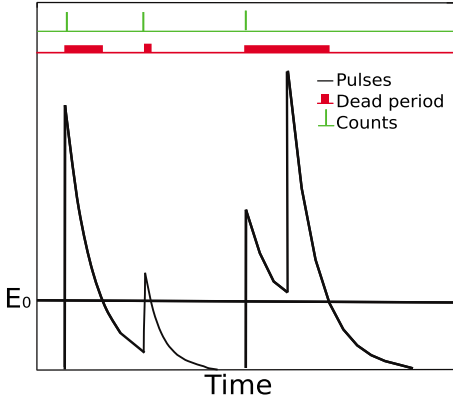
Figure 2. Sketch of dead time loss.

Figure 4. The solid curve is the sum of the paralyzation curves for the four brightest LADs, each of which is shown as a dashed curve.

short time scale ($\ll 1$ μs) with amplitude proportional to the energy deposited by the photon (E_p). The pulse will then decay exponentially ($V(t) = V_p e^{-t/\alpha}$ corresponding to $E(t) = E_p e^{-t/\alpha}$) with a signal decay time α, while the electronics reads out the pulse. The LAD cannot register a new photon until the previous pulse is reduced to the reset level, expressed as energy, E_0. On the other hand, if a photon hits the detector before the previous signal is reduced to its reset level, the new photon is not registered. This effect results in dead time losses. Figure 2 shows a sketch of how the pulses and counts occur in a detector. The bold red area marks the time when the detector is dead. Green ticks show when a pulse is registered as a count. The last pulse occurs before the reset level is reached and is therefore not counted.

[20] On the basis of preflight data, *Grefenstette et al.* [2008] determined $\alpha = 0.75$ μs and $E_0 = 5.5$ keV. No error bars were given; 0.75 μs is three times the fluorescence
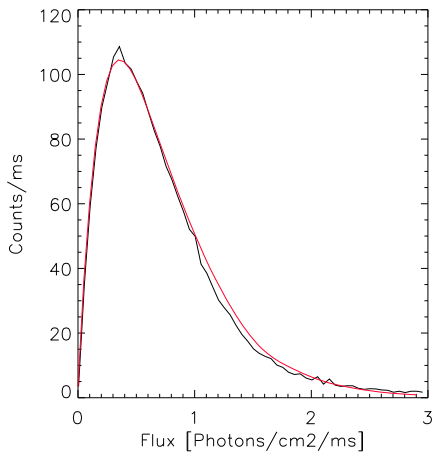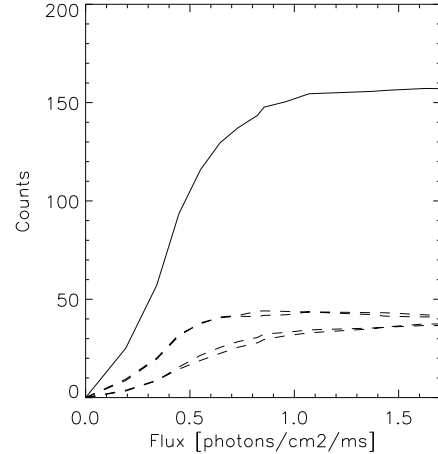
decay time of NaI scintillator, which is the scintillator used in the BATSE LADs. It can be argued that the decay time should be shorter, and in that case the dead time effects will be slightly less. However, we here assume the decay time from *Grefenstette et al.* [2008]. A discussion of how a change in the decay time influences the results is given in section 3.

[21] A paralyzable detector with dead time, which does not vary on the photons' energy, suffers from dead time losses on the form

$$m = ne^{-n\tau} \tag{3}$$

where m is the measured count rate, n is the incoming pulse rate, and τ is the instrument's dead time [*Knoll*, 1989]. In our simulation we use equation (2), with $\alpha = 0.75$ μs and $E_0 = 5.5$ keV to calculate τ for each pulse or sequence of pulses (see Figure 2). With the input distribution of photons in energy and time we can vary the total number of incoming photons, i.e., the photon flux, and calculate the number of pulses by the DRM and then simulate what will be measured by BATSE. Figure 3 shows the paralyzation curve of equation (3) with a dead time of 3.3 μs in red and the result of our MC dead time simulation when the pulse rate increases. The x axis is the photon flux, and the y axis is the counts per ms. The input in the MC simulation a given number of 500 keV photons uniformly distributed in time (within 1 ms). This sample plot illustrates that for a given number of detected counts, e.g., 60, there are two possible incoming photon flux values, 0.1 and 0.9 photons/cm^2/ms. However, all the short-duration single-peaked TGFs in this study are on the left side of the maximum. Figure 4 shows the paralyzation curve for TGF 2955, where the spectral and temporal distributions from our simulation are included. The solid curve is combined of the four LADs facing the TGF. The dashed curves represent each of the four LADs. Two of the LADs have a larger effective area and therefore reach the

Figure 3. The paralyzation curve for equation (3) (red) and MC (black).
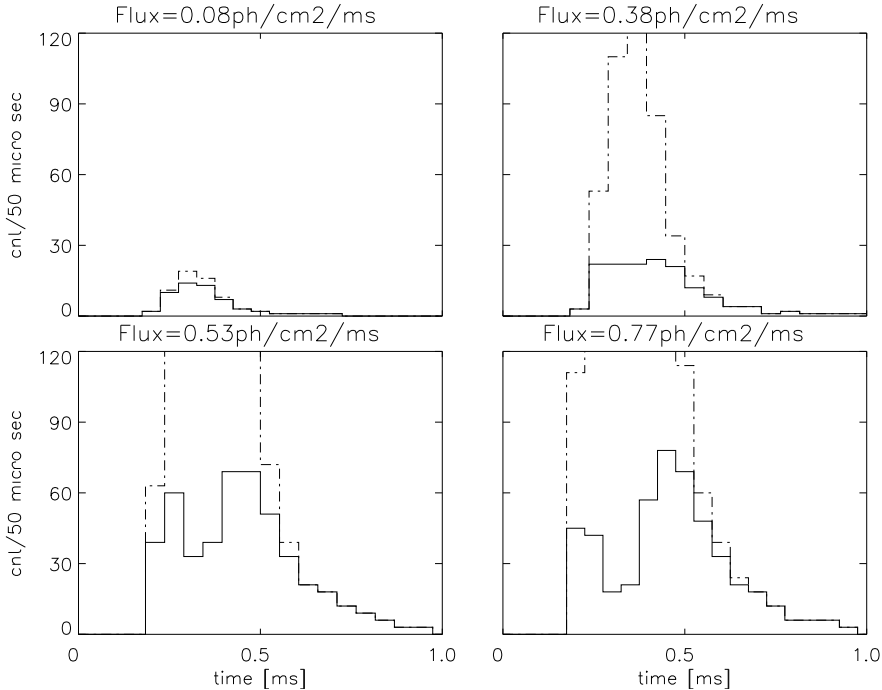
Figure 5. Light curves of a simulated TGF for various incoming photon fluxes. The light curves of pluses created in the LAD are dashed, and the counts in the LAD taking dead time losses into account are shown in solid.

maximum before the two others. The x axis unit is the average flux during the TGF. The y axis unit is the total number of counts per TGF when the incoming photons are folded through the DRM and scaled for dead time losses. Figure 5 shows the resulting light curves for various fluxes (given in the header of each panel). The dashed light curves describe the pulses created in one LAD, and the solid curves are counts with dead time effects included. As the flux approaches the value which gives the maximum in the paralyzation curve (1 photon/cm^2/ms), a single-peaked pulse–light curve transforms into a double-peaked counts–light curve. If the TGF's counts–light curve does not have this single-to-double transition form, then it must be on the left side of the maximum.

[22] Step 5: Determine the production altitude and incoming flux using χ^2 test. Østgaard et al. [2008] created a library of Monte Carlo simulated TGFs escaping the atmosphere with various initial assumptions. The library is now modified with the slightly different initial assumptions as already described in section 2. For all the modeled TGFs in our library [Østgaard et al., 2008] we have followed steps 1 to 4. For each modeled TGFs we have also varied the total number of photons. Each of the TGFs are first converted from photons to pulses and then to counts to get an estimate of the measured counts in the four LADs facing the TGF. These estimates are then compared with what BATSE measured in the four LADs with most counts to create a χ^2

between the simulated and the measured TGFs. This calculation leads to a 3-D matrix of χ^2 with spectral index varied from 1.0 to 1.5, altitudes varying from 10 to 30 km and incoming photon number varying from 50 to 1050 photons per TGF where the TGF production duration is from step 1.

[23] Figure 6 (left) shows the χ^2 values of altitude and spectral index with an incoming photons flux of 0.51 photons/cm^2/ms. Figure 6 (right) shows the χ^2 values of altitude and various number of incoming photons fluxes with a constant spectral index 1.0. The degrees of freedom is three (four energy channels). For BATSE TGF 2955 the best fit is an altitude of 23 km with a spectral index of 1.0 and an average incoming photons flux of 0.51 photons/cm^2/ms. The energy spectrum of TGF 2955 is shown in black in Figure 7 (top). The simulated TGF folded through the DRM and corrected for dead time is shown in red in Figure 7.

[24] Step 6: Check if the photon distribution that gave the best fit in production altitude and spectral index also reproduces the observed time delay. After determining the production altitude, spectral index, and the incoming photon flux of the TGF we check the temporal properties by calculating the time delay for the best fit TGF and compare it with the measurements. Figure 7 (bottom) shows the light curve of TGF 2955 and the best-fit simulated TGF, with the corresponding time delay. The time delay is calculated from
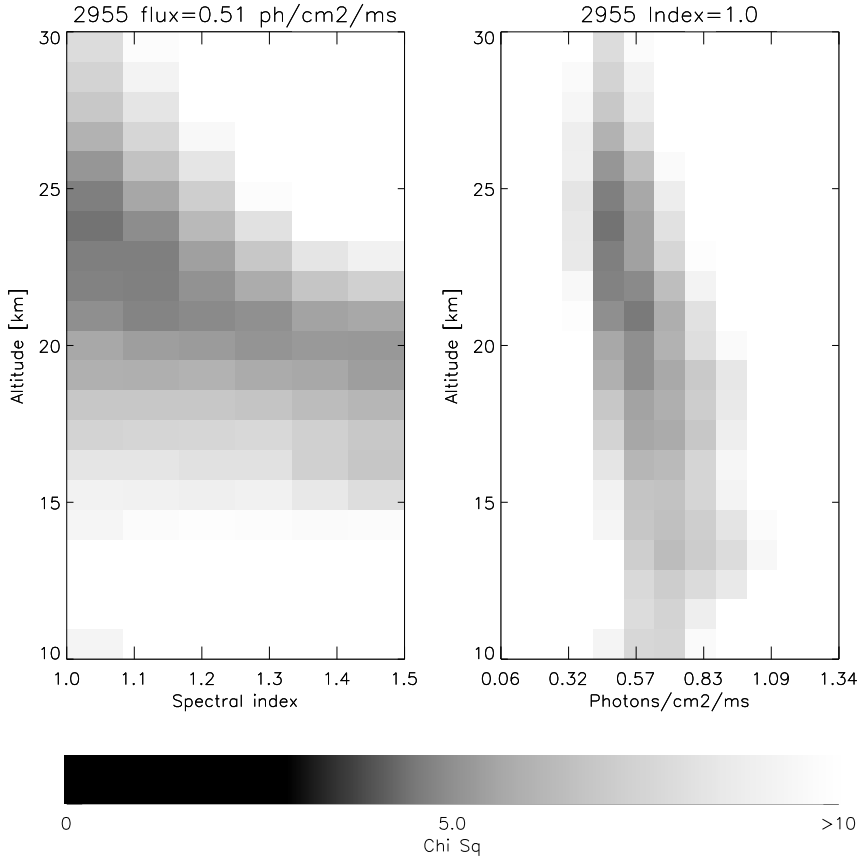
Figure 6. The χ^2 calculated for various production altitudes, spectral indexes, and fluxes. Altitude versus (left) spectral index and (right) average flux.

the light curves of hard and soft photons, where the division is set to 300 keV. The light curves are binned in 25 uniformly logarithmically distributed time bins ranging from 10 to 100 μs, and we use the mean of the minimums from the cross-correlation functions for each time bin size as the time delay. This method is described by *Feng et al.* [2002]. The light curve of TGF 2955 (Figure 7, bottom left) and our modeled TGF (Figure 7, bottom right) are shown. The time delay in our modeled TGF without taking dead time into account is 38 ± 18 μs. When the dead time effects are included, the time delay increases to 118 ± 16 μs. The measured time delay is 145 ± 40 μs.

[25] Step 7: Verifying the zenith angle. An initial assumption in this analysis was that the zenith angle calculated from the relative counts that were measured in each of the four brightest LADs. From equation (3) and Figure 3 it is clear that if the detector is totally paralyzed, the LAD that is hit by most photons may not be the LAD that has the most counts. In such cases the calculated zenith angle would be wrong. However, if we are on the left (lower) side of the peak

of the paralyzation curve, in all four LADs, the dead time effects can be corrected and we can reestimate the zenith angle. For all the single-peaked TGFs analyzed in this study the change in zenith angle is less than 10°, which is the angle binning used for our modeled spectra in the library.

[26] Finally, we can also calculate the total number of pulses created in BATSE. The dead time ratio, R, is the ratio between pulses and counts.

$$R = \frac{n_{\text{pulses}}}{n_{\text{counts}}}, \qquad (4)$$

and describes how many times brighter, than measurements from BATSE, TGFs are. For TGF 2955 the dead time ratio is 3.77.

3. Results

[27] During its lifetime, BATSE recorded 76 TGF events. The BATSE TGFs have three different time profiles: (1) the
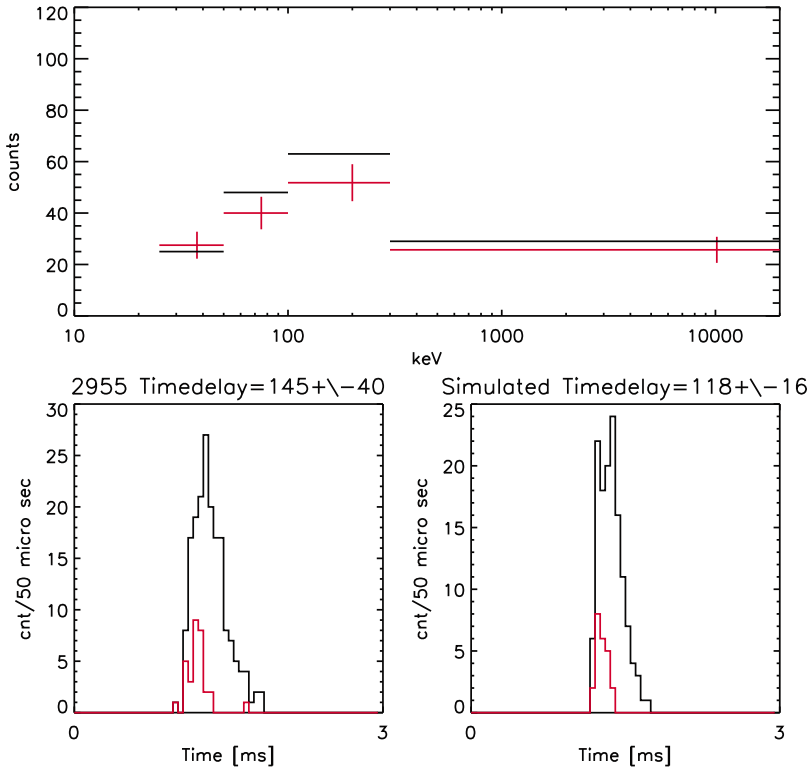
Figure 7. (top) Energy spectrum of BATSE TGF 2955 in black and a simulated TGF from 23 km altitude with a spectral index 1.0 in red. (bottom) Light curves of (left) BATSE TGF 2955 and (right) the simulated TGF light curve. The black curve is the total light curve (channel 1 to 4), and the red curve is the light curve of channel 4. The time delays given in the headers are between channel 1 to 3 and channel 4 in μs.

single-peaked TGFs; (2) the multipeaked TGFs, which contain two or more separate peaks during the event; and (3) the long duration bursts, which are events that last for several milliseconds. As already shown under step 5 in section 2, the TGFs that are measured as single peaks must be single peaks of incoming photons as well. Furthermore, for these TGFs we are confident that the LADs are not paralyzed, and we are on the left and lower side of the peak in Figure 4. For these TGFs the dead time losses can be corrected for.

[28] We have identified five short-duration, single-peaked TGFs that comply with this criterion. For each of them we have preformed the seven steps as described in section 2 to give an altitude, incoming flux, and time delay. We have also studied one double-peaked TGF that may be a result of dead time losses and will be shown and discussed in section 4. This method can also be used on multipeaked TGFs. However, we find that the number of counts in each peak in these cases was too low (<5 counts per channel per peak) to preform a χ^2 analysis.

[29] Table 1 summarizes the results for the five TGFs that have been reanalyzed by using the libraries with beamed spectra and isotropic within a 50° cone. From Table 1 it is clear that the production altitude is reduced when taking dead time into account both for the beamed and isotropic libraries. For TGF 5587 the dead time losses are small, and the results from *Østgaard et al.* [2008] still hold. The given uncertainties in production altitude are where the values of the χ^2 array are increased by ≤1 from its minimum.

[30] In the result presented in Table 1 we used $\alpha = 0.75$ μs and $E_0 = 5.5$ keV in equation (2). To see how the dead time effects vary with a different decay time, we did the same analysis with varying α. For $\alpha = 0.5$ μs we found the same production altitude, but the best fit was found at lower incoming photon fluxes. An increase in the dead time will reduce the maximum number of counts a detector can measure. With $\alpha = 1.0$ μs the number of counts in our simulation was significantly lower than in the BATSE TGFs, and consequently, the χ^2 value increases and was

Table 1. Time Delay and Production Altitude[a]

BATSE		Beamed					Cone				Duration
TGF	TD (μs)	Ø (km)	New (km)	TD (μs)	Flux	R	New (km)	TD (μs)	Flux	R	(μs)
2144	125 ± 22	39	17 ± 3	148 ± 22	0.62	3.72	25 ± 3	162 ± 22	0.62	4.52	266
2370	124 ± 18	40	16 ± 4	117 ± 21	0.36	3.08	22 ± 2	96 ± 12	0.36	3.30	222
2465	147 ± 19	26	21 ± 4	137 ± 20	0.49	3.68	24 ± 2	124 ± 17	0.49	4.38	208
2955	145 ± 40	39	22 ± 4	118 ± 16	0.51	3.77	26 ± 2	80 ± 21	0.51	3.77	237
5587	66 ± 34	14	12 ± 1	52 ± 17	0.20	1.46	29 ± 15	54 ± 17	0.28	2.11	555

[a]From *Østgaard et al.* [2008] (Ø) and this study (new) with the beamed and the cone case. The listed flux is the average flux of photons (ph/cm^2/ms) of the TGF. R is the dead time ratio calculated by equation (4). The calculated initial duration of TGFs are shown under the "Duration" column. TD, time delay.

found to be >10 in all TGF. Therefore, the decay time in the BATSE instrument must be ≤1.0 μs.

4. Discussion

4.1. Why Are the Production Altitudes Reduced?

[31] From Table 1, it is clear that the production altitude is significantly reduced when the dead time effects are included in the analysis. All of the single peak TGFs are now between 12 km and 23 km compared to 14 to 40 km from *Østgaard et al.* [2008]. These new altitude estimates are also in agreement with earlier studies [*Dwyer and Smith*, 2005; *Williams et al.*, 2006; *Carlson et al.*, 2007]. We will now discuss how the dead time effects leads to a softer spectrum and consequently a higher estimated production altitude than when dead time effects are included in the analysis.

[32] Figure 8 shows the relationship between the calculated spectral index and the dead time ratio, R, which is derived from equation (4). The spectral index is not the spectral index of the initial TGF spectrum at the production altitude, but the spectral index from a best-fit obtained power law curve of the LADs for energy channels in our simulation after folding the simulated TGF (same as in section 2) through the DRM and scaling it for dead time losses. As the losses due to dead time increase, the measured energy spectrum gets softer. This is a result of the Compton time-delayed tail, shown in Figure 5. The high-energy photons arrive mostly at the peak intensity time of the TGF, the time when the dead time losses are the most significant, while the softer Compton scattered photons arrive later and do not suffer from as much dead time losses. This was also shown by *Grefenstette et al.* [2008].

[33] In simulations performed by *Østgaard et al.* [2008] we showed that TGFs have a softer energy spectrum for increasing production altitudes. The same result is also shown in simulations by *Dwyer et al.* [2008] and *Carlson et al.* [2007]. Therefore, if the TGF suffers from significant dead time losses (i.e., appears softer than they should), an analysis of TGFs without taking dead time losses into account would result in a higher production altitude than an analysis taking this effect into account.

[34] Our results (shown in Table 1) give lower production altitude for beamed case than for the cone case. This is the opposite of results from *Dwyer and Smith* [2005] and *Carlson et al.* [2007]. Both these studies use all photons, out to angles consistent with the satellites' detection thresholds, which escapes the atmosphere in their spectral analysis. In our study we divide our spectra in observation angles. For the beamed case all TGF are observed outside the pro-

duction cone, while in the cone case all TGF are observed inside the production cone. *Østgaard et al.* [2008] showed that the energy spectrum is significantly softer when observed outside the production cone than inside. Also, modeled TGFs have a softer energy spectrum when produced at increasing altitudes. Therefore, to fit a given observed spectrum at a given angle, the modeled beamed case implies a lower altitude than the modeled cone case.

4.2. Why Do Dead Time Effects Lead to Larger Time Delays?

[35] The observed time delay in the TGFs is a result of Compton scattering in the atmosphere and dead time losses. *Grefenstette et al.* [2008] showed that dead time losses will increase the time delay in measured TGFs, and the same result is found in this study. High-energy photons arrive at the beginning of the TGF, and as the intensity increases, dead time losses become more significant. The scattered photons, which are reduced in energy, arrive at later times in the TGF. The result of dead time will therefore reduce the number of late arriving high-energy photons and the early arriving low-energy photons, which leads to a longer separation of the hard and the soft light curve. Figure 9 shows how the time delay increases with increasing dead time ratio. The time delay increases rapidly as the dead
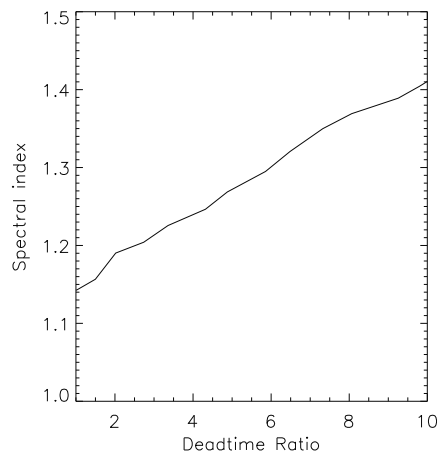

Figure 8. Best-fit power law spectral index of a simulated TGF when dead time effects are included as a function of the dead time ratio from equation (4).
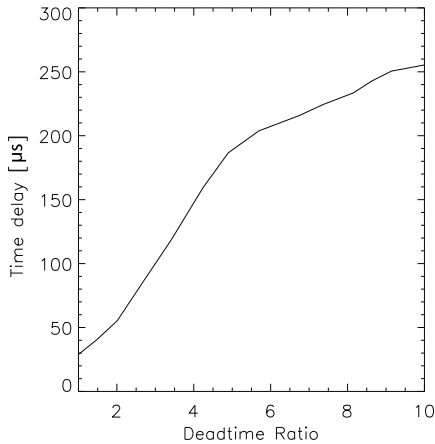
Figure 9. Time delay in simulated TGFs as a function of the dead time ratio from equation (4).

time ratio increases. In the work of *Østgaard et al.* [2008] our simulations showed that the time delay increases as the production altitude decreases. This pattern is not likely to be found in measurements that suffer from dead time losses. The effect of dead time loss on the time delay is greater than the effect of decreasing TGF production altitude. For TGFs of equal intensity produced at different altitudes, high-altitude TGFs will experience less attenuation and will therefore at satellite altitudes have a higher flux, which results in a longer time delay.

[36] As the dead time losses are not significant because of low count rate at the beginning and at the end of the TGFs, these losses do not influence our estimate ($\pm 2\sigma$) of the total duration time. Dead time losses are only important at the peak intensities and even if the peak is increased by a factor of four, the $\pm 2\sigma$ does not change.

4.3. Double Peaks

[37] As shown in step 4 in section 2, a single-peaked TGF can become a double-peaked TGF if the measurements suffer from significantly dead time losses. Most of the multipeaked TGFs have a longer separation between the peaks (>1 ms) than what can be explained by dead time. However, the light curve of TGF 2348 has two peaks separated by ~200 μs. From Figure 5 we have shown that one effect of dead time losses is that a single-peaked TGF can be measured as a double-peaked TGF. By increasing the input flux in our simulation we can reproduce this temporal behavior. In Figure 10 the total (black) and hard ($E > 300$ keV) (red) light curve is shown for TGF 2348 and a TGF from our MC. Both the measured and simulated TGFs have more high-energy counts in the first peak. Since the TGFs gets softer with time, this is what we would expect if dead time losses divide the peak. In the "single-peaked measured as a double" case the dead time ratio for this TGF is ~6. Because of the high incoming photon flux, we have passed the peak of the paralyzation curve (see Figure 4), and we are not able to discuss the spectral properties of TGF 2348. We cannot rule out the possibility that TGF 2348 is actually a double-peaked TGF. In that case the dead time losses are significantly lower than if it is a single-peaked TGF measured as a double.

4.4. Dead Time Effects for Different Types of TGFs

[38] Because of the long trigger window (64 ms), a short event such as a TGF (which typically last 1 ms) needs to be very intense to cause a trigger. Several of the BATSE TGFs contain several peaks, each lasting approx 1 ms. On the basis of the same argument, we would assume that single-peaked TGFs suffer from more dead time losses than the multipeaked TGFs. From these considerations it is likely that all the multipeaked TGFs as well as the long-duration events also are on the left and lower side of the paralyzing peak in Figure 4, and consequently, the dead time losses can be corrected. This argument is also used by *Dwyer et al.* [2008] where five long-duration BATSE events, which
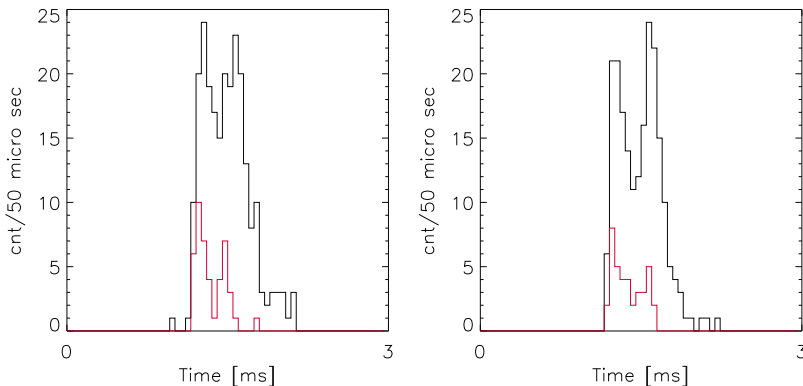

Figure 10. The light curve of (left) BATSE TGF 2348 and (right) simulated TGF. The black curve is the total light curve (channel 1 to 4), and the red is the light curve of channel 4.

were suggested to be electrons and not X-rays entering the detectors, were studied.

4.5. Duration of the Production Mechanism for TGFs

[39] As a side effect of this study, we have also found the initial duration of the TGFs. The duration times, as calculated in step 1, are listed in Table 1. Of the five single-peak TGFs we have analyzed, four have an initial duration time of 200–270 μs, while TGF 5587 has an initial duration of 555 μs. This time scale must reflect the duration of the production mechanism of TGFs.

5. Summary

[40] By modeling the propagation of X-rays through the atmosphere and the interaction of each photon with detector material until it is (or not) detected as a count by the read-out electronics, we have reanalyzed five single peak TGFs and found the following:

[41] 1. TGFs that suffer from significant dead time losses ($R = 3$–4) have a lower production altitude than analyses without dead time. A reanalyzes of five short-duration single-peaked TGFs which in the work of Østgaard et al. [2008] were determined to be produced at 26 to 40 km altitude are now reduced to lower altitudes (14–22 km). One TGF, which has lower dead time losses ($R = 1.46$), was determined to be produced at 12 km altitude in this study and 14 km in the work of Østgaard et al. [2008].

[42] 2. The dead time losses increase the time delay between the hard and the soft photons of the TGF, in agreement with earlier results [Grefenstette et al., 2008]. When we account for dead time losses we could reproduce the large time delays which are found in the BATSE TGFs measurements. In this analysis we have found consistent between production altitude and time delay.

[43] 3. The analyzed single-peaked TGFs have dead time ratio up to 4, confirming earlier results [Grefenstette et al., 2008].

[44] 4. We have shown that the double peak of TGF 2348 may be a result of dead time losses. We have shown that a single-peaked TGF can turn into a double-peak TGF. If this TGF is a single-peaked TGF measured as a double, it is ~6 times brighter than measured by BATSE.

[45] 5. In step 1 (described in section 2) we have calculated the duration of the production process of TGF on the basis of the light curve of high-energy photons. This time scale (200 to 600 μs) must reflect the duration of the production mechanism of TGFs.

References

Carlson, B. E., N. G. Lethinen, and U. S. Inan (2007), Constraints on terrestrial gamma ray flash production from satellite observation, *Geophys. Res. Lett.*, 34, L08809, doi:10.1029/2006GL029229.

Carlson, B. E., N. G. Lethinen, and U. S. Inan (2009), Terrestrial gamma ray flash production by lightning current pulses, *J. Geophys. Res.*, 114, A00E08, doi:10.1029/2009JA014531.

Chanrion, O. A., and T. Nubert (2008), A pix-cc code for simulation of streamer propagation in air, *J. Comput. Phys.*, 15, 7222–7245, doi:10.1016/j.jcp.2008-016.

Cohen, M. B., U. S. Inan, and G. Fishman (2006), Terrestrial gamma ray flashes observed aboard the compton gamma ray observatory/burst and transient source experiment and elf/vlf radio atmospherics, *J. Geophys. Res.*, 111, D24109, doi:10.1029/2005JD006987.

Cummer, S. A., Y. Zhai, W. Hu, D. M. Smith, L. I. Lopez, and M. A. Stanley (2005), Measurements and implications of the relationship between lightning and terrestrial gamma ray flashes, *Geophys. Res. Lett.*, 32, L08811, doi:10.1029/2005GL022778.

Dwyer, J. R., and D. M. Smith (2005), A comparison between Monte Carlo simulations of runaway breakdown and terrestrial gamma-ray flash observations, *Geophys. Res. Lett.*, L22804, doi:10.1029/2005GL023848.

Dwyer, J. R., B. W. Grefenstette, and D. M. Smith (2008), High-energy electron beams launched into space by thunderstorms, *Geophys. Res. Lett.*, 35, L02815, doi:10.1029/2007GL032430.

Feng, H., T. Li, M. Wu, M. Zha, and Q. Q. Zhu (2002), Temporal and spectral properties of gamma-ray flashes, *Geophys. Res. Lett.*, 29(3), 1036, doi:10.1029/2001GL013992.

Fishman, G. J., et al. (1994), Discovery of intense gamma-ray flashes of atmospheric origin, *Science*, 264, 1313–1316, doi:10.1126/science.264.5163.1313.

Grefenstette, B. W., D. M. Smith, J. R. Dwyer, and G. J. Fishman (2008), Time evolution of terrestrial gamma ray flashes, *Geophys. Res. Lett.*, 35, L06802, doi:10.1029/2007GL032922.

Gurevich, A. V., and K. P. Zybin (2001), Runaway breakdown and electric discharges in thunderstorms, *Phys. Uspeki*, 44, 1119–1140, doi:10.1070/PU2001v044n11ABEH000939.

Inan, U. S., and N. G. Lehtinen (2005), Production of terrestrial gamma-ray flashes by an electromagnetic pulse from a lightning return stroke, *Geophys. Res. Lett.*, 32, L19818, doi:10.1029/2005GL023702.

Inan, U. S., S. C. Reising, G. J. Fishman, and J. M. Horack (1996), On the association of terrestrial gamma-ray bursts with lightning and implications for sprites, *Geophys. Res. Lett.*, 23(9), 1017–1020.

Inan, U. S., M. B. Cohen, R. Said, D. M. Smith, and L. I. Lopez (2006), Terrestrial gamma-ray flashes and lightning discharges, *Geophys. Res. Lett.*, 33, L18802, doi:10.1029/2006GL027085.

Knoll, G. (1989), *Radiation Detection and Measurements*, John Wiley, New York.

Lehtinen, N. G., M. Walt, U. S. Inan, T. F. Bell, and V. P. Pasko (1996), γ-ray emission produced by a relativistic beam of runaway electrons accelerated by quasi-electrostatic thundercloud fields, *Geophys. Res. Lett.*, 23, 2645–2648, doi:10.1029/96GL02573.

Moss, G., V. P. Pasko, N. Liu, and G. Veronis (2006), Monte Carlo model for analysis of thermal runaway electrons in streamer tips in transient luminous events and streamer zones of lightning leaders, *J. Geophys. Res.*, 111, A02307, doi:10.1029/2005JA011350.

Nemiroff, R. J., J. T. Bonnell, and J. P. Norris (1997), Temporal and spectral characteristics of terrestrial gamma ray flashes, *J. Geophys. Res.*, 102, 9659–9666, doi:10.1029/96JA03107.

Østgaard, N., T. Gjesteland, J. Stadsnes, P. Connell, and B. Carlson (2008), Production altitude and time delays of the terrestrial gamma flashes: Revisiting the burst and transient source experiment spectra., *J. Geophys. Res.*, 113, A02307, doi:10.1029/2007JA012618.

Roussel-Dupre, R. A., A. V. Gurevich, T. Tunnel, and G. M. Milikh (1994), Kinetic theory of runaway breakdown, *Phys. Rev. E*, 49, L06802, doi:0.1103/PhysRevE.49.2257.

Smith, D. M., L. I. Lopez, R. P. Lin, and C. P. Barrington-Leigh (2005), Terrestrial gamma-ray flashes observed up to 20 mev, *Science*, 307(5712), 1085–1088, doi:10.1126/science.1107466.

Stanley, M. A., X. M. Shao, D. M. Smith, L. I. Lopez, M. B. Pongratz, J. D. Harlin, M. Stock, and A. Regan (2006), A link between terrestrial gamma-ray flashes and intracloud lightning discharges, *Geophys. Res. Lett.*, 33, L06803, doi:10.1029/2005GL025537.

Williams, E., et al. (2006), Lightning flashes conducive to the production and escape of gamma radiation to space, *J. Geophys. Res.*, 111, D16209, doi:10.1029/2005JD006447.

P. H. Connell, Institute of Mechanical Science, University of Valencia, Calle Tenor Alonso 55, Valencia, E-46110, Spain. (paul.connell@uv.es)

G. J. Fishman, NASA Marshall Space Flight Center, VP 62, Huntsville, AL 35812, USA. (fishman@msfc.nasa.gov)

T. Gjesteland, N. Østgaard, and J. Stadsnes, Department of Physics and Technology, University of Bergen, Allegt 55, N-5007 Bergen, Norway. (thomas.gjesteland@uib.no; nikolai.ostgaard@uib.no; johan.stadsnes@ift.uib.no)